Meas. Sci. Technol. **9** (1998) 1142–1151. Printed in the UK PII: S0957-0233(98)88561-5

Highly accurate non-contact characterization of engineering surfaces using confocal microscopy

H-J Jordan†, M Wegner and H Tiziani

Universität Stuttgart, Institut für Technische Optik, Pfaffenwaldring 9, 70569 Stuttgart, Germany

Received 21 October 1997, accepted for publication 13 March 1998

Abstract. Optical non-contact techniques are very interesting for 3D characterization of sensitive and complex engineering surfaces. Unfortunately, the application of optical techniques was for many years restricted to selected types of surfaces which have only moderate variations of height and surface slope relative to their lateral resolution and measurement field. Owing to the fact that artefacts and form deviations occur with high spatial frequencies in optically measured topographs, there were some difficulties in interpreting the results and comparing them with the tactile standard techniques for surface characterization. Furthermore, artefacts in optically measured profiles have often been misinterpreted in terms of the resolution of optical techniques being higher than that of the tactile techniques. This paper presents two optical methods of confocal microscopy for highly accurate characterization of surfaces. The first method works on measurement fields of less than 1 mm^2 and is in practice absolutely comparable to the mechanical stylus instrument, even on rough surfaces. For this method results compare very well not only in surface statistics but also in topographic raw data, as will be demonstrated for the PTB roughness standards. The second method works on measurement fields up to square centimetres.

Keywords: scanning confocal microscopy, non-contact 3D characterization of complex engineering surfaces, PTB roughness standards, comparison of optical and tactile techniques for surface analysis, microlens arrays in confocal microscopy

1. Introduction

In recent years, the technique of confocal microscopy, first described by Minski in 1957 [1, 2], has become a more and more powerful tool for surface characterization, in parallel with the development of computer-based image processing systems. The basic principle of confocal microscopy (Minski named it double focusing microscopy) is shown in figure 1. Light emitted from a point light source (for example a laser beam focused onto an illumination pinhole) is imaged onto the object focal plane of a microscope objective MO (the first focusing). A specimen location in focus leads to a maximum flux of light through the detector pinhole (the second focusing), whereas light from defocused object regions is partly suppressed.

The depth-discriminated detector signal, limited by the pinhole size, is reduced strongly when defocusing the specimen [3, 4]. This results in optical sectioning and enhancement of contrast by suppression of light scattered from defocused specimen locations. A further advantage of confocal microscopy against classical light microscopy is that the lateral resolution is significantly greater (by about 20%) [5]. In addition, the effect of optical sectioning allows the determination of the specimen's z coordinate.

Various designs of confocal microscopes for the acquisition and evaluation of 3D topographic data are possible. Time-consuming serial x–y scanning techniques have been developed for the acquisition of depth-discriminated sections in confocal laser scanning microscopes. A further z scan is necessary to acquire all the data for the evaluation of 3D topographic maps [6, 7].

Recent applications of these types of confocal microscopes are in biological and medicinal cell analysis [8] and the analysis of smooth engineering surfaces [9–11]. An overview of applications of confocal microscopy is given in [12, 13]. Common to all these applications is the use of highly magnifying microscope objectives with high numerical apertures ($0.6 < NA < 1.4$) which allow only small object volumes.

This paper describes two methods of parallel x–y scanning video techniques applying confocal microscopy for ultra-precise optical 3D measurements of engineering surfaces. The first method is using a multiple pinhole mask (a Nipkow disc) in an intermediate image plane of a microscope as first described by Petran *et al* [14].

† Present address: NanoFocus Messtechnik GmbH, Bismarckstraße 120, 47057 Duisburg, Germany.

0957-0233/98/071142+10$19.50

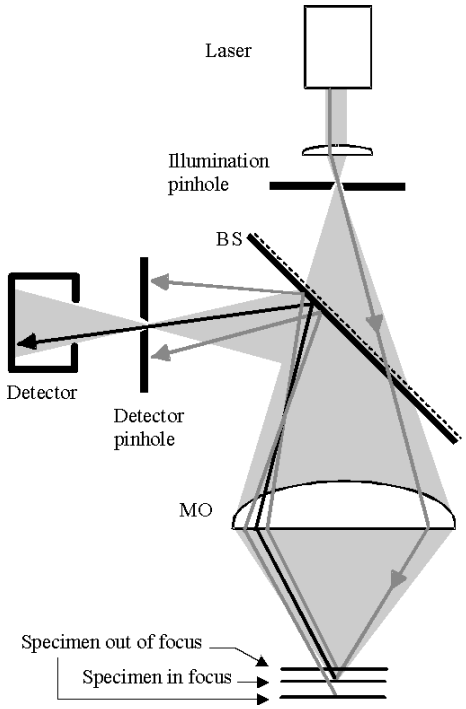

Figure 1. The basic principle of confocal microscopy.

Combined with CCD image processing, the rotating Nipkow disc effects a real-time x–y scan of the object field. Just an additional z scan is necessary for 3D topometry. The use of microscope objectives with medium numerical apertures enables parallel x–y scanning of depth-discriminated sections in object fields up to 1 mm^2. This technique of scanning confocal microscopy (SCM) makes fast and accurate 3D topometry for analysis of the roughness of complex engineering surfaces possible [15–17], as will be demonstrated in this paper.

The second method, named microlens array confocal microscopy (MLACM) is suitable for object fields up to square centimetres [18, 19]. This technique makes precise optical 3D analysis of forms and microstructures possible.

2. The depth response $I(z)$ and full width at half maximum *(FWHM)*

A comprehensive description of the theory of confocal microscopy is given in [5]. Some formulae relevant to 3D topometry are as follows.

The depth response $I(z)$ of a confocal system is proportional to a sinc^2 function,

$$I(z) = \left(\frac{\sin[kz(1-\cos\alpha)]}{kz(1-\cos\alpha)} \right)^2 I_0 \qquad (1)$$

which depends on the aperture angle α of the microscope objective, the wavelength of light λ, the wavenumber $k = 2\pi/\lambda$ and the coordinate of defocusing z. Significant for the depth response $I(z)$ is the full width at half maximum, which is

$$FWHM = 2z_{1/2} \approx \frac{0.443\lambda}{1-\cos\alpha}. \qquad (2)$$

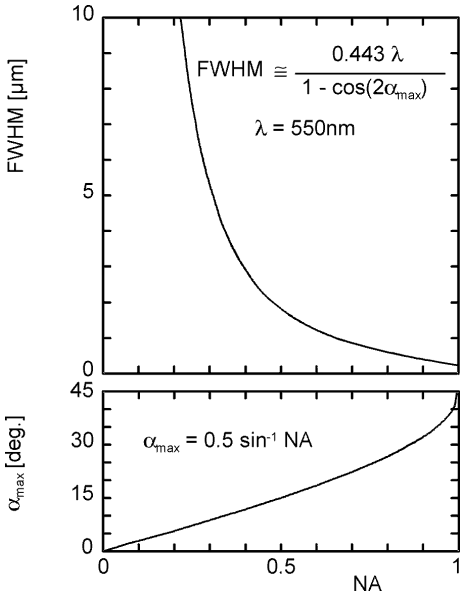

Figure 2. Graphs of the full width at half maximum of the confocal depth response (equation (2)) and of the maximum surface slope for specular reflection (equation (3)) versus the numerical aperture.

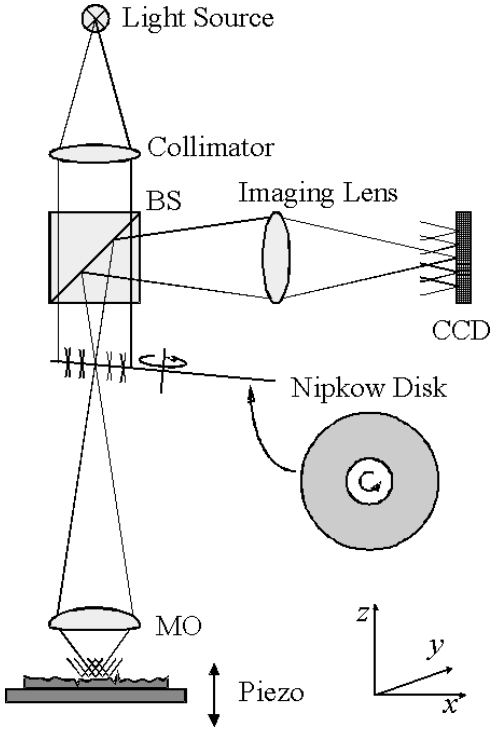

Figure 3. The SCM set-up, using a rotating Nipkow disc.

The half angle of the numerical aperture NA determines the maximum surface slope

$$\alpha_{max}^{spec} = 0.5 \sin^{-1} NA \qquad (3)$$

for specular reflection at a microscopic smooth surface element of the specimen. The wavelength and the numerical aperture determine the *FWHM* of the depth response $I(z)$ of the detector's intensity.

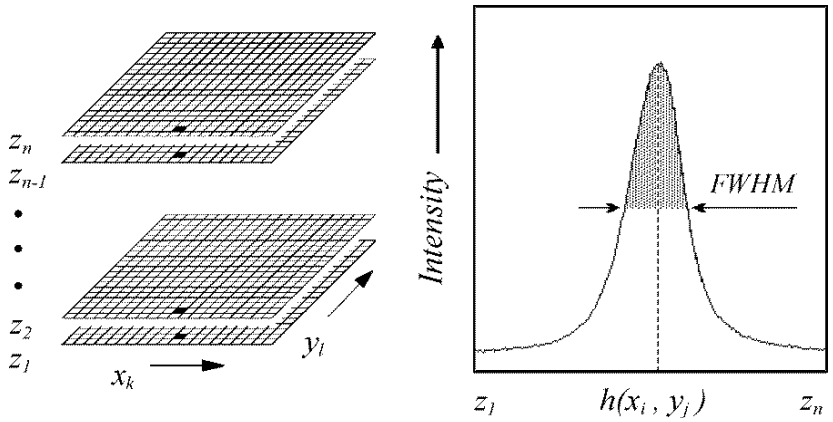

Figure 4. The evaluation of the topography. Calculation of the height coordinate $h(x_i, y_j)$ as the centre of the depth response $I(x_i, y_j, z)$ for each pixel of the stack z_1 to z_n.

Table 1. Parameters of the SCM set-up for various microscope objectives.

	Leica NPL Fluotar 20×/0.45	Leica NPL Fluotar 50×/0.85	Leica PL 160×/0.95
Working distance (μm)	2000	220	70
α_{max}^{spec} (degrees)	13.4	29.1	35.9
$FWHM_{Theory}$ (μm)	2.3	0.51	0.35
$FWHM_{Experiment}$ (μm)	6.1	1.1	0.52
Height resolution (nm)	40	20	10
Airy resolution at λ = 0.55 μm (μm)	0.75	0.4	0.35
Typical measurement field	565 μm × 576 μm	226 μm × 230 μm	70 μm × 72 μm
Typical pixel resolution	(1.1 μm)^2	(0.44 μm)^2	(0.14 μm)^2

Engineering surfaces often have (more or less) microroughness within the probe spot size. Therefore, diffuse reflection increases the maximum surface slope which can be measured ($\alpha^{diff} \geq \alpha_{max}^{spec}$) and α_{max}^{spec} indicates a lower limit of the surface slope.

When one is using a Nipkow disc microscope, a decrease of the numerical aperture *NA* increases the object field for the real-time x–y scan. For a 20×/0.45 microscope objective the calculated *FWHM* is about 2.3 μm (the upper graph in figure 2), whereas the measured *FWHM* was about 6.1 μm [16]. Calculating the topographic height $h(x_i, y_i)$ by determining the centre of gravity of the depth response $I(z)$ like in equation (4) improves the height resolution down to fractions of the *FWHM*. Using a 20× magnification of the microscope objective allows object fields of up to 1 mm^2. The numerical aperture *NA* limits the surface slope to $\alpha_{max}^{spec} \approx 14^\circ$ (the lower graph in figure 2) which by experience is sufficient for most engineering surfaces.

3. Scanning confocal microscopy (SCM)

For x–y scanning of a depth-discriminated section we use a Nipkow disc, which consists of pinholes of 20 μm diameter, separated by 200 μm and arranged in a spiral shape [10, 11]. The rotating disc is illuminated by a plane wave and acts as a scanning multiple-point light source, which is imaged onto the object focal plane of the microscope objective MO (figure 3). Backwards, after the reflection or scattering of light at the specimen, each (illuminating) Nipkow pinhole acts as its own detector pinhole. The depth-discriminated x–y information $I(x, y, z)$ is imaged onto a CCD camera (HITACHI KP-160, 1/2″ sensor with 699 (horizontal) × 576 (vertical) pixels, sensitivity of 0.05 lux on the chip). Thus, during one rotation of the disc, an x–y section of the specimen is acquired on video in real time. By an additional z scan (PI piezo, 60 μm expansion) of the specimen, a stack z_1 to z_n ($n = 32/64/128/256$) of depth-discriminated CCD camera frames is acquired, from which a 3D topography can be constructed with a resolution of about 1% ($n = 256$) of the *FWHM* [15–17].

Figure 4 shows a depth response $I(x_i, y_j, z)$ measured on a ground surface using a 20×/0.45 objective. Figure 4 also shows the mode of evaluation of the height coordinate $h(x_i, y_j)$ as the centre of $I(x_i, y_j, z)$. A well formed depth response according to equation (1) is decisive for accurate confocal 3D topometry, especially for applications using microscope objectives of medium numerical aperture *NA*.

For alignment of this system one has to concentrate on reliability, smoothness, ambiguity and areal homogeneity of the system's depth response $I(z)$. The topographic height $h(x_i, y_i)$ is obtained by determining the centre of gravity

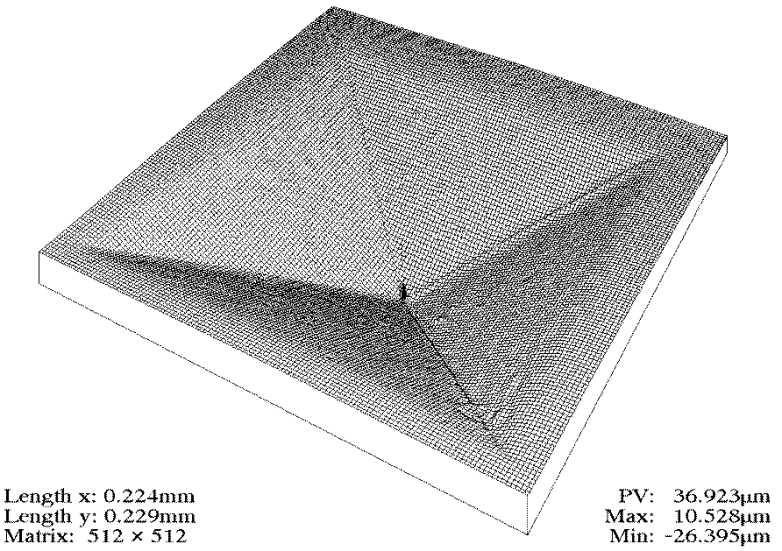

Figure 5. An isometric plot of a 3D data set of a Vickers hardness dent, measured with the SCM.

of $I(z)$ as indicated in figure 4:

$$h(x_i, y_j) = \mathrm{d}z \frac{\sum_{z_k \in FWHM} I(x_i, y_j, z_k) z_k}{\sum_{z_k \in FWHM} I(x_i, y_j, z_k)}. \qquad (4)$$

Image processing and height evaluation were done using a 512 × 512 pixel framegrabber and a 66 MHz 486 computer. For $n = 256$ depth-discriminated x–y sections, the total time for data acquisition and height evaluation was 4 min. A typical object field is of the order of $(565\ \mu\mathrm{m})^2$ using a 20× objective with a numerical aperture of 0.45 ($\alpha_{max}^{spec} = 13.4^\circ$). Thus, the lateral pixel resolution for this magnification is about 1 μm. The lateral optical resolution of a confocal microscope is improved by about 20% relative to the classical Airy disc criterion. Thus, using a 20× objective, the lateral pixel resolution is close to the lateral optical resolution of about 0.6 μm. The corresponding height resolution Δz for the $20\times/0.45$ objective is 40 nm for $n = 256$ height sections at the maximum piezo expansion of 60 μm, measured on a tilted mirror of $\lambda/20$ flatness, which was in practice flat within the SCM measurement field size. The height resolution Δz is the RMS deviation of the measured data set. Using a $160\times/0.95$ objective ($\alpha_{max}^{spec} = 35.9^\circ$), a typical field of view is of the order of $(70\ \mu\mathrm{m})^2$. In this configuration, the lateral optical resolution of about 0.3 μm was fully obtained by the lateral pixel resolution of 0.14 μm. The corresponding height resolution Δz for the $160\times/0.95$ objective is 10 nm, measured on a mirror as described above. Physical parameters of the SCM set-up for various microscope objectives are summarized in table 1.

4. Experimental results using the SCM

Extensive investigations of the accuracy and resolution of the SCM set-up have been performed. Some of them were using *a priori* information about the 3D structure of test pieces such as a Vickers hardness test. Detailed investigations have been performed using several PTB roughness standards. These standards have been designed and calibrated by the *Physikalisch Technische Bundesanstalt* (PTB) in Braunschweig, Germany. They are periodic and one-dimensionally rough, which means that the surface profile varies only in one direction with a period of 4 mm. The PTB standards allow detailed analysis of the height as well as the lateral resolution and accuracy of profilometer systems. They can also be used to analyse the capability of optical topometers to reproduce varying local surface slopes. In our opinion this is the most important problem to be solved, especially in establishing

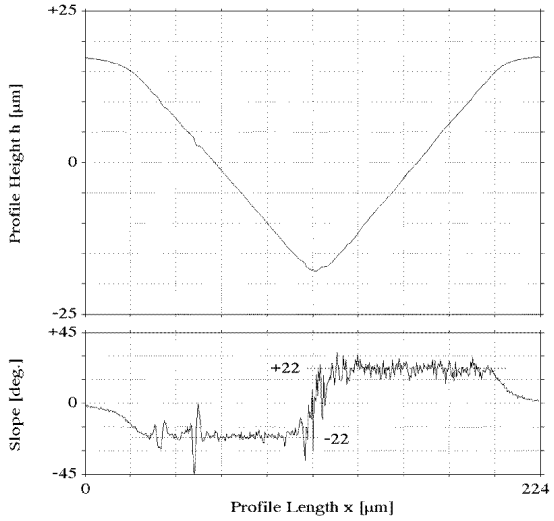

Figure 6. The profile through the centre of the Vickers dent (figure 5) and the corresponding surface slope of the profile.

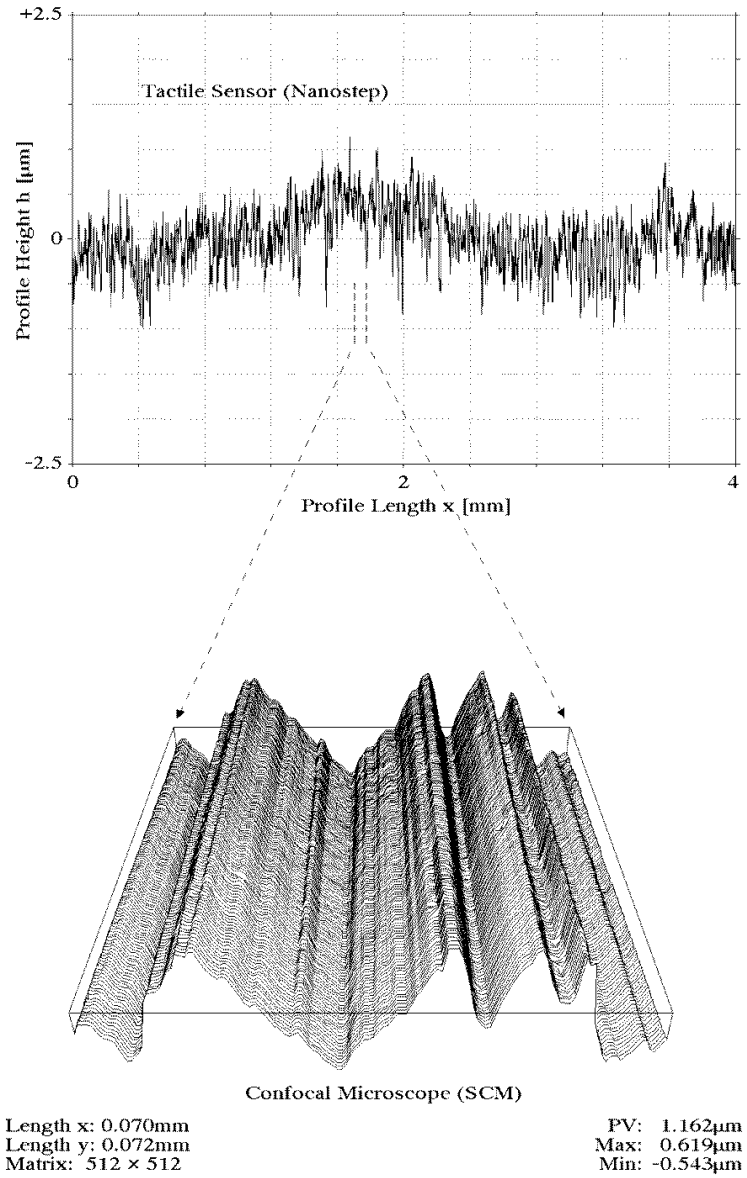

Figure 7. The profile of a PTB roughness standard (fine) measured with the Nanostep (upper graph) and an isometric plot of a 3D data set measured with the SCM (lower graph).

optical systems as an alternative to tactile systems for analysis of rough surfaces. To give a solution to this very important problem, tactile measurements have been carried out for comparison after our SCM measurements had been completed. These tactile measurements have been made at the PTB using a Nanostep stylus instrument from Rank Taylor Hobson with a tip radius of 0.1 μm. It should be noticed that all presentations within this paper are showing raw data of the relevant systems. No artefacts or spikes have been filtered out in any plot.

4.1. Vickers hardness tests

For a Vickers hardness test a square diamond pyramid with an aperture angle of 136° is pressed into the specimen with a defined force. The depth and therefore the diameter of the dent are functions of the hardness of the specimen.

Figure 5 is an isometric 3D plot of results for such a hardness test. The topography of figure 5 has been measured using a $50\times/0.85$ microscope objective at an object field of 224 μm $\times$ 229 μm. The depth of the dent is of the order of 35 μm. The upper part of figure 6 shows a profile through the centre of the 3D data set and the lower part of figure 6 shows the corresponding graph of the surface slope as the derivative of the profile. Owing to the aperture angle of 136° between opposite flanks of the diamond pyramid, the slope of opposite profile flanks of the dent should be $\pm 22°$. This is confirmed by the lower part of figure 6.

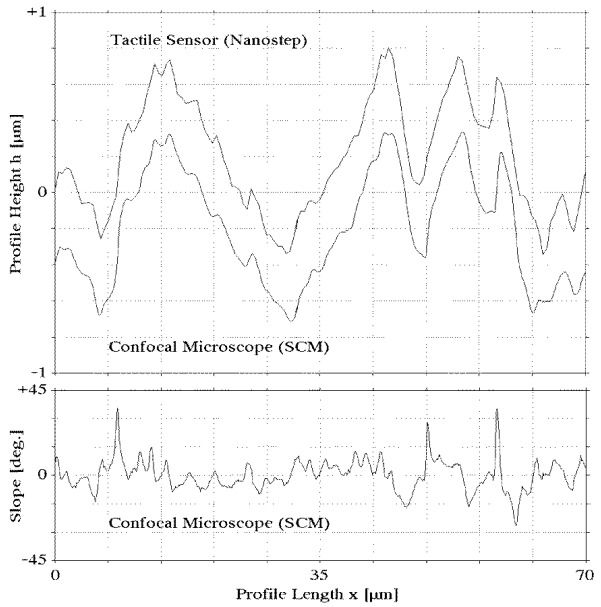

Figure 8. A comparison of a profile of the PTB standard measured with the SCM and the corresponding part of the Nanostep profile from figure 7 (upper graph). The surface slope, corresponding to the SCM profile (lower graph).

4.2. The PTB roughness standard (fine)

The roughness data of this one-dimensional rough standard are $R_a = 0.201$ μm, $R_z = 1.55$ μm and $R_{max} = 1.84$ μm (DIN 4768) with respective uncertainties of $\pm 8\%$, according to the certificate of calibration. The upper part of figure 7 shows a profile measured with the tactile Nanostep system at the PTB. The profile is dominated by profile amplitudes of about 0.5 μm and spatial periods of a few micrometres. Specimens with roughness of this type are in general difficult to measure with optical techniques.

A highly resolved topographic measurement has been performed using a $160\times/0.95$ microscope objective at an object field of 70 μm $\times$ 72 μm. The 3D presentation of this topography and its location with respect to the tactile measured profile are shown in the lower part of figure 7. This presentation also shows the one-dimensionality of the roughness. A detailed comparison of these two measurements is shown in figure 8. The upper part of figure 8 shows a detail of the tactile profile of figure 7, according to the location of the SCM topography together with the centre row profile of the SCM topography. The maximum difference between these two profiles is of the order of 100 nm and the average difference is of the order of a few nanometres. Thus, the comparability of tactile and optical profilometry [20] has been improved greatly. The lower part of figure 8 presents the slope derived from the SCM profile. The maximum slope was measured to be about 37°.

4.3. The PTB roughness standard (coarse)

The roughness data of this standard are $R_a = 1.45$ μm, $R_z = 7.24$ μm and $R_{max} = 9.6$ μm (DIN 4768) with respective uncertainties of $\pm 4\%$, according to the certificate of calibration. Figure 9 shows an unfiltered top of view grey-scale presentation of a measurement performed with the $20\times/0.45$ microscope objective of the SCM system at an object field of 835 μm $\times$ 575 μm. Again the one-dimensionality of the roughness standard can clearly be recognized. Figure 9 also shows the location of the centre row profile (R 256) of figure 10. In order to make a full length profile comparison between results of the SCM technique and tactile systems over the standard's period of 4 mm, a set of nine lateral partly displaced SCM measurements was performed. The overlap between neighbouring topographs was eliminated and one SCM macroprofile was created, as demonstrated in figure 11. A comparison of the SCM macroprofile with a profile obtained with the Nanostep system is presented in figure 12. The upper part of figure 12 shows a stylus profile record of the PTB. The lower part of figure 12 shows the SCM macroprofile. The deviation of the roughness parameters calculated from this SCM macroprofile from those calculated from the stylus profile record was of the order of less than 1%. It can be seen from figure 12 that the confocal profile record compares well with the stylus profile record. This means that the SCM set-up is suitable for precise 3D topometry of rough engineering surfaces, with resolution and accuracy in the 10 nm range.

4.4. The LASERTEX sheet

As an example for 3D analysis of complex engineering surfaces having roughness as well as form, a highly resolved topograph of an aluminium LASERTEX sheet is presented in figure 13. This surface has plateaux of nearly unique height (bright areas in figure 13) with very steep slopes down to the valleys (dark areas in figure 13), as can be seen from the profile in figure 14. The steepest slopes of this surface have been measured to be about 65°. The light scattered back from the steep slopes due to the microroughness of the highest spatial frequencies was sufficient for accurate topometry. It should be noticed that no spike filtering was applied to all the results presented in this paper. The roughness of the profile of column 160 (figure 14) is approximately seven times the roughness of the profile of column 256, which does not cross any plateaux. This demonstrates the need for accurate 3D topometry of rough engineering surfaces.

In the SCM set-up we developed, the measured field size is limited by the magnification of the microscope's objective to be less than 1 mm^2 using a $20\times$ microscope objective with $NA = 0.45$. To overcome the limitation in the field size another approach of the confocal technique was developed using microlens arrays.

5. Microlens array confocal microscopy (MLACM)

In co-operation with the imaging lens, each microlens of the ML array in figure 15 acts as a single confocal microscope [18, 19, 21], like the basic set-up of a confocal microscope (figure 1). Thus the confocal technique is parallelized using

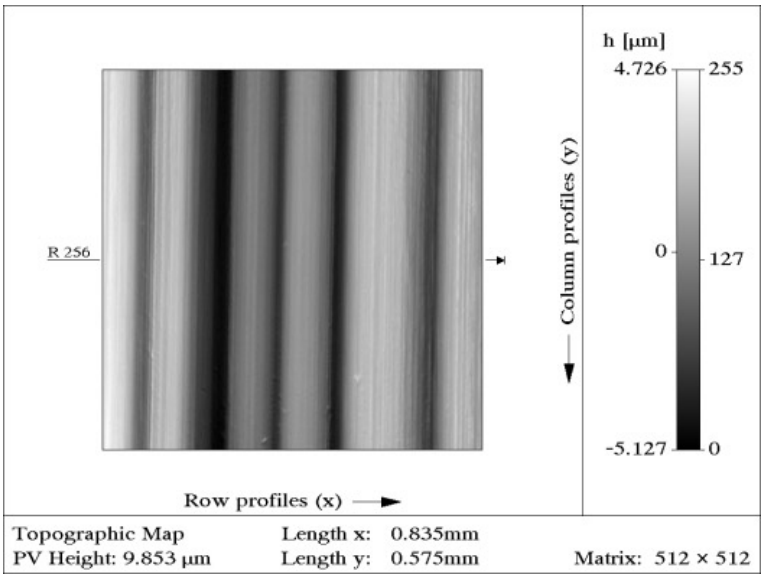

Figure 9. The 3D data set of a PTB standard (coarse) in a top of view grey-scale presentation, measured with the SCM.

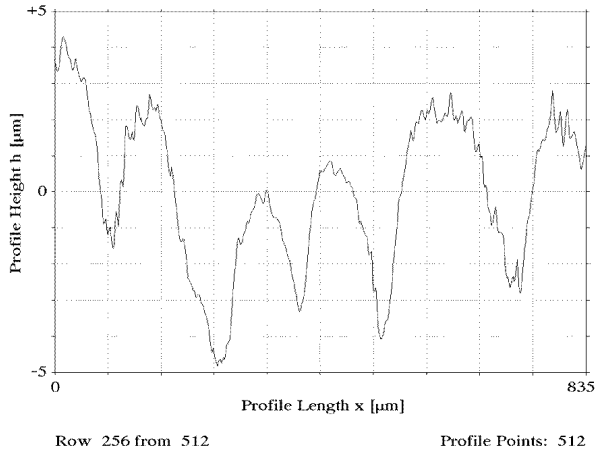

Figure 10. The centre row profile of the 3D data set from figure 9.

an ML array. The depth response $I(z)$ and the *FWHM* of the MLACM are determined by the *NA* of a single microlens and are furthermore given by equation (1) and equation (2). However, the object field size is now limited by the size of the microlens array and no longer by the properties of a single microlens. Object fields of square centimetres are now possible.

6. Experimental results using the MLACM

Because the microlens array replaces the x–y scanning properties of the rotating Nipkow disc, just a z scan (PI piezo, 180 μm expansion) of the specimen has to be carried out for the acquisition of the stack z_1 to z_n of depth-discriminated height sections. Like in the SCM, the height map of a MLACM topography is evaluated from equation (4). Image processing was equivalent to that for the SCM, using 512 × 512 pixels. Typical data of the

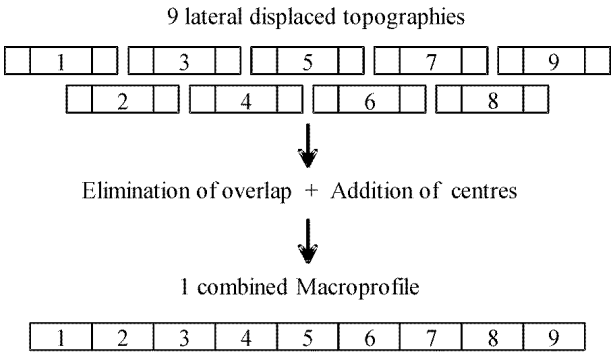

Figure 11. The principle of constructing a macroprofile.

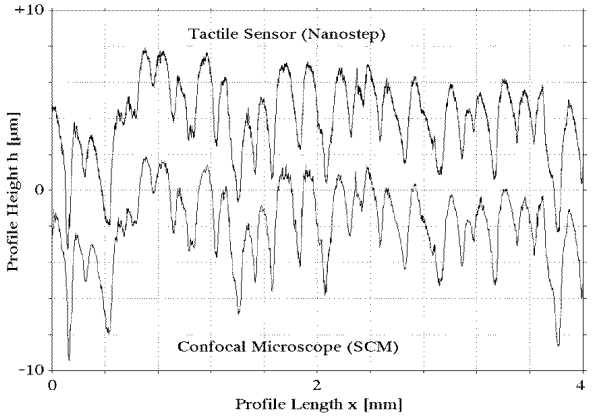

Figure 12. A comparison of an unfiltered stylus profile record (Nanostep, 0.1 μm tip radius) and the unfiltered confocal macroprofile (SCM, 20×/0.45 MO) using a PTB standard (coarse).

microlens arrays are focal lengths of 250 μm, numerical apertures of 0.3 and diameters of 150 μm for the individual microlenses.

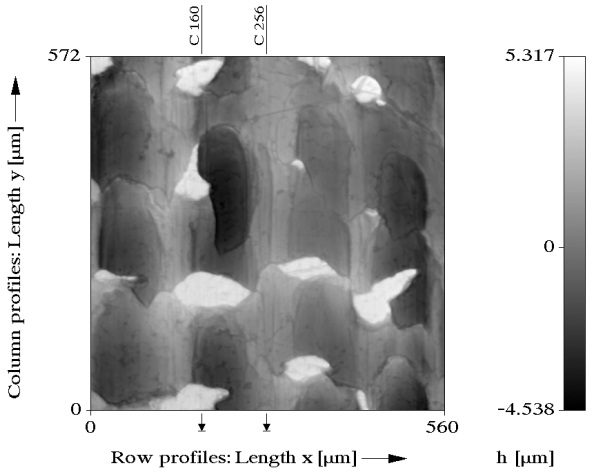

Figure 13. Top of view grey-scale presentation of a 3D topograph (raw data) of a LASERTEX sheet, measured with the SCM (20×/0.45 microscope objective).

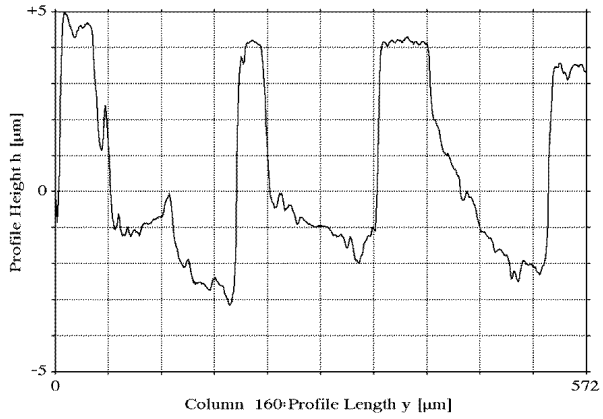

Figure 14. The profile of column 160 of the 3D data set from figure 13.

6.1. The Canadian 10 cent coin

Figure 16 shows a 3D topograph of a Canadian 10 cent coin. Because the object field for this measurement was $(11\ \mathrm{mm})^2$ and the diameter of a single microlens was 150 μm, the topograph shows about 74×74 relevant height values, each covering 7×7 image pixels. This is the basic sampling interval of the MLACM. However, there is a way to improve and adapt the sampling interval to the requirements. The technique is the other way round, relative to the construction of the macroprofile (figure 11). Here, after the acquisition of a first sub-topograph, the specimen is laterally displaced by a fraction of a microlens diameter. Now the next sub-topograph is acquired and so on. After the acquisition of all sub-topographs, the resulting topograph is constructed by interlacing of all sub-topographs. With this procedure, resulting MLACM topographs with an improved sampling interval are obtained. In figure 17, 7×7 sub-topographs have been obtained in order to construct a data set with 512×512 relevant height values, each covering an improved sampling interval of just 1 pixel. For this example, the

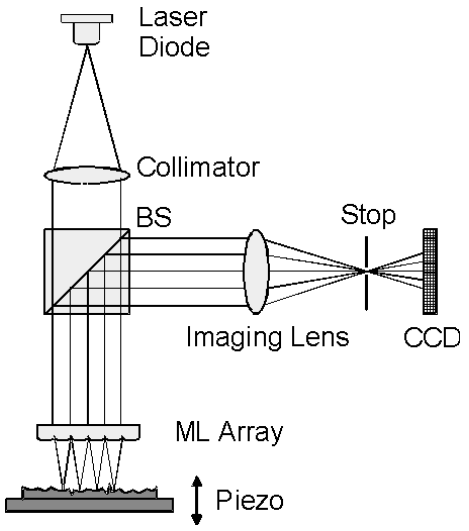

Figure 15. The MLACM set-up, introducing microlens arrays into confocal microscopy.

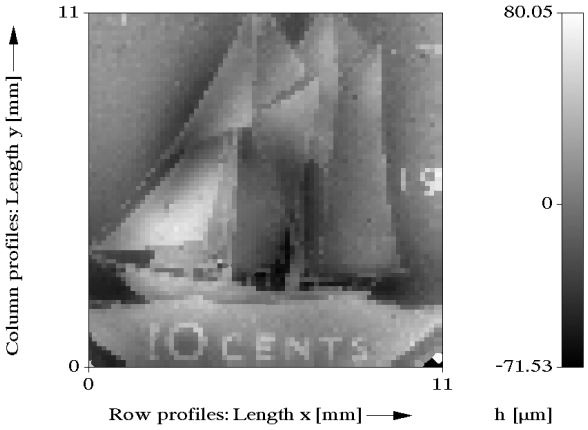

Figure 16. Top of view grey-scale presentation of a 3D topograph of a Canadian 10 cent coin. This example shows the basic sampling interval of the MLACM.

improved sampling interval of about $\Delta x \approx \Delta y \approx 21.5\ \mu$m is still large compared with the diffraction-limited size of a microlens focus of about 1.5 μm. Even fine details like single ropes of the shrouds of the ship have been resolved.

6.2. A spherical grating

Figure 18 shows a 3D topograph of a grating of 600 μm period. This data set was measured with the improved sampling interval technique. The grooves of the grating have a depth of about 23 μm and a spherical shape, as can be seen from the profile and the corresponding slope in figure 19. A maximum slope of about 12.5° was measured, which exceeds the maximum slope for specular reflection $\alpha_{max}^{spec} \approx 8.7°$ ($NA = 0.3$) by 43%, due to diffuse reflection.

6.3. Leather

Figure 20 shows a a 3D topograph of leather, a highly complex type of surface. The grey-scale presentation shows

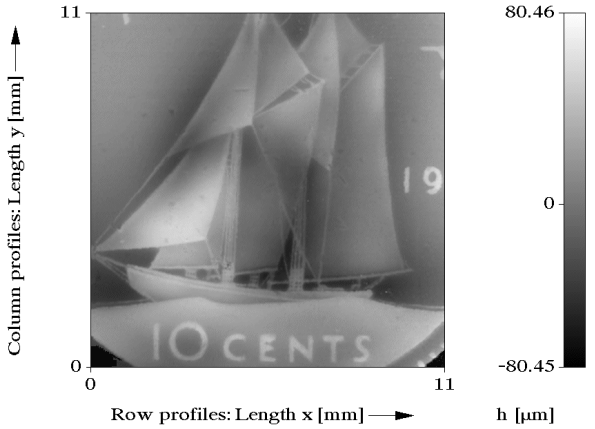

Figure 17. Top of view grey-scale presentation of a 3D topograph of the Canadian 10 cent coin with the improved sampling interval.

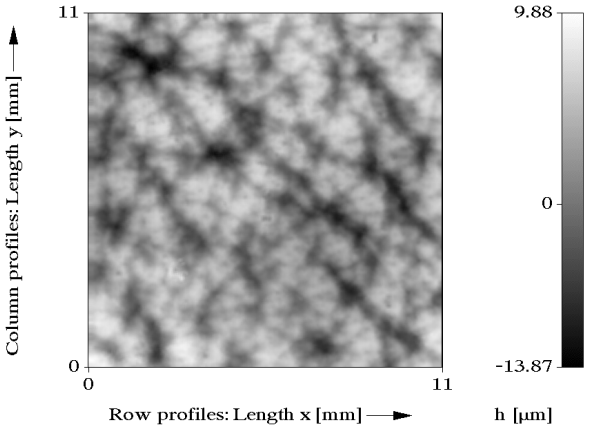

Figure 20. Top of view grey-scale presentation of a 3D topograph of leather. Again, this data set was measured with the improved sampling interval technique.

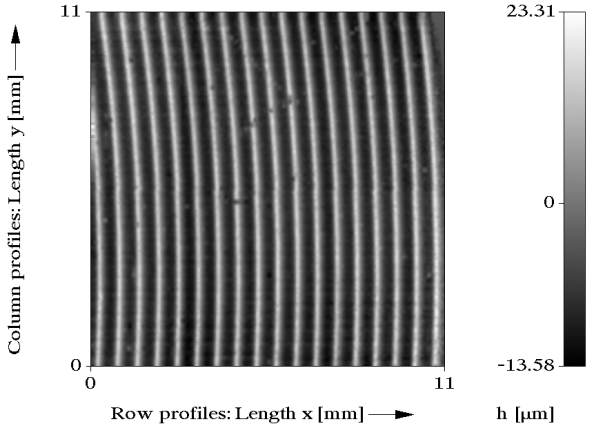

Figure 18. Top of view grey-scale presentation of a 3D topograph of a grating of 600 μm period. This data set was measured with the improved sampling interval technique.

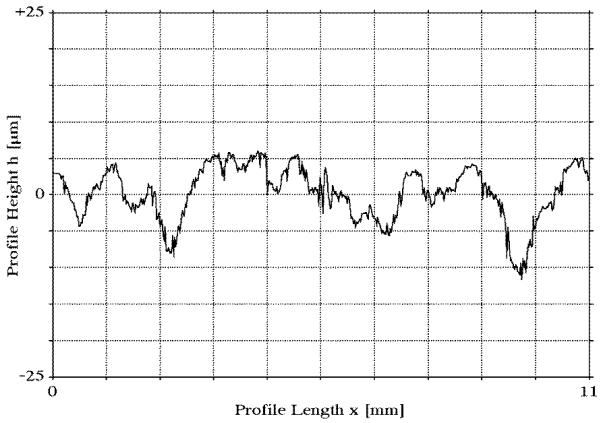

Figure 21. The centre row profile of the 3D data set from figure 20. The profile exhibits both form and microgeometry, probably from pores.

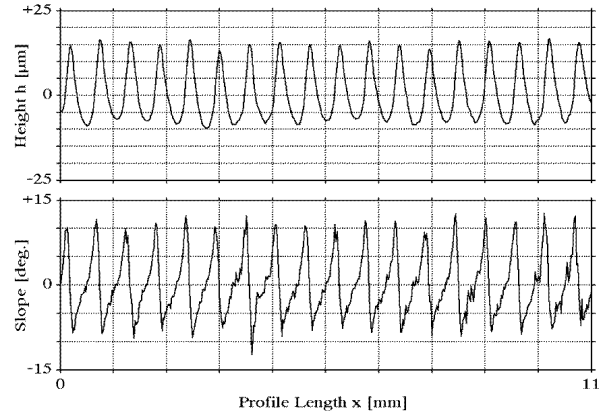

Figure 19. The centre row profile of the 3D data set from figure 18. The grooves of the grating have a depth of about 23 μm and a spherical shape, as can be seen from the profile and the corresponding slope.

primarily the macroscopic form of the leather. However, due to the improved sampling interval, microgeometry probably from pores can be seen in figure 21.

7. Conclusions

The technique of scanning confocal microscopy has demonstrated its capability for fast and highly accurate non-contact 3D surface characterization up to object fields of 1 mm^2, even for rough engineering surfaces. The results obtained (raw data topographs as well as surface statistics) compare very well with those obtained by using tactile standard techniques. Thus, the SCM is a powerful alternative to tactile techniques.

The technique of microlens array confocal microscopy extends object fields to square centimetres, allowing accurate non-contact 3D form measurements. Thus, topographs of engineering surfaces of some (10 μm)^2 up to square centimetres can be measured accurately using confocal microscopy.

Acknowledgments

The authors gratefully acknowledge the European Commission, the Deutsche Forschungsgemeinschaft and the Bundesministerium für Bildung, Forschung und Technologie

for their financial support of various projects on confocal microscopy and also Dr Hillmann/PTB, Labor für Oberflächen, for supporting us with stylus profile records.

References

[1] Minsky M 1961 Microscopy apparatus, USA patent 3013467 (filed 1957)
[2] Minsky M 1988 Memoir on inventing the confocal scanning microscope *Scanning* **10** 128–38
[3] Hamilton D K, Wilson T and Sheppard C J R 1981 Experimental observation of the depth-discrimination properties of scanning microscopes *Opt. Lett.* **6** 625
[4] Wilson T 1989 Depth response of scanning microscopes *Optik* **81** 113
[5] Wilson T 1990 *Confocal Microscopy* (New York: Academic)
[6] Hamilton D K and Wilson T 1982 Three-dimensional surface measurement using the confocal scanning microscope *Appl. Phys.* B **27** 211
[7] Carlsson K and Åslund N 1987 Confocal imaging for 3-D digital microscopy *Appl. Opt.* **26** 3232
[8] Massig J H, Preissler M, Wegener A R and Gaida G 1994 Real-time confocal laser scan microscope for examination and diagnostics of the eye *in vivo Appl. Opt.* **33** 690
[9] Hamilton D K and Wilson T 1982 Surface profile measurement using the confocal microscope *J. Appl. Phys.* **53** 5320
[10] Xiao G Q and Kino G S 1987 A real-time confocal scanning optical microscope *Proc. SPIE* **809** 107
[11] Xiao G Q, Corle T R and Kino G S 1988 Real-time confocal scanning optical microscope *Appl. Phys. Lett.* **53** 716
[12] Hellmuth T 1993 Neuere Methoden in der konfokalen Mikroskopie *Phys. Blätter* **49** 489
[13] Dixon A J, Doe N and Pang T-M 1987 Industrial applications of confocal scanning optical microscopy *Proc. SPIE* **809** 37
[14] Petran M, Hadravsky M, Egger M D and Galambos R 1968 Tandem-scanning reflected-light microscope *J. Opt. Soc. Am.* **58** 661
[15] Tiziani H J and Jordan H-J 1995 Contributions to *Optical Non-Contact Techniques for Engineering Surface Metrology* BCR Information, European Commisson, Report EUR 16161 EN
[16] Jordan H-J 1996 Optische Mikrotopometrie und Rauheitsmessung an technischen Oberflächen *Berichte aus dem Institut für Technische Optik der Universität Stuttgart* (Stuttgart: Institute for Applied Optics, University of Stuttgart)
[17] Jordan H-J, Wegner M and Tiziani H 1997 Optical topometry for roughness measurement and form analysis of engineering surfaces using confocal microscopy *Progress in Precision Engineering and Nanotechnology, Proc. 9th Int. Precision Engineering Seminar/4th Int. Conf. on Ultraprecision in Manufacturing Engineering* vol 1, ed H Kunzmann *et al* (Braunschweig: Physikalisch-Technische Bundesanstalt) p 171
[18] Tiziani H J and Uhde H M 1994 Three-dimensional analysis by a microlens-array confocal arrangement *Appl. Opt.* **33** 567
[19] Tiziani H J and Uhde H M 1994 Three-dimensional image sensing by chromatic confocal microscopy *Appl. Opt.* **33** 1838
[20] Hillmann W (submitted by Kunzmann H) 1990 Surface profiles obtained by means of optical methods – are they true representations of the real surface? *Ann. CIRP* **39** 581
[21] Tiziani H J, Achi R, Krämer R N and Wiegers L 1996 Theoretical analysis of confocal microscopy with mirolenses *Appl. Opt.* **35** 120